



The Large Near-Field Enhancement due to Strong Coupling Between the LSP on the Metal Coupled Nanodisks and on the Gold Film for Short Attosecond Pulse Generation

Nasrin Shahnavaz¹ · Masoud Mohebbi¹

Received: 7 September 2020 / Accepted: 16 November 2020 / Published online: 26 November 2020
© Springer Science+Business Media, LLC, part of Springer Nature 2020

Abstract

Within a mid-IR few-cycle laser, the generation of MHz isolated attosecond pulses via nanoplasmonic field enhancement in a structure that consisted of a metal coupled nanoparticle-disk, an insulator spacer, and a thin metal film is theoretically investigated. The interaction between the localized surface plasmons caused by the coupled nanodisks and the metal layer results in increased electric field. The resonance wavelengths of these two types of surface plasmons supported by the nanostructure are tailored by changing the coupled nanoparticle-disk size and the material type. Numerical calculations are used to optimize nanostructure and attain plasmonic field enhancement factors up to 86. The HHG process is studied by the time–frequency analysis. Our studies show that only short trajectories contribute to HHG and also, the chirp of these harmonics is very low. As a result, an isolated 40 as pulse without phase compensation is obtained directly by superposing the chirp-free high-order harmonics.

Keywords Localized surface plasmons · High-order harmonic generation · Attosecond pulse generation

Introduction

One of the nonlinear phenomena that occurs with short and strong laser radiation interactions with atoms and molecules is high-order harmonic generation. High-order harmonic generation is of great interest due to its applications in X-ray production, coherent attosecond pulses, and lithography [1]. The physical mechanism of high-order harmonic generation for a single atom or molecule can be described through a three-step model [2]. In the first step, the electron is released by tunneling ionization through the potential barrier to the continuum state. In the second phase, the electron accelerates away from the nucleus and returns when the sign of electric field changes. In the later stage, the electron is recombined with the nucleus and releases the additional kinetic energy gained by irradiating a high harmonic photon. An interesting way to produce high-order harmonics is to

use metallic nanostructures [3–6]. When nanostructures are irradiated with low intensity laser field, the plasmonic mode coupling of nanostructures and laser field enhances the laser field. The resonance wavelength of the surface plasmons depends on the size and shape of the nanoparticles as well as the dielectric environment around it [7]. If the field amplification is large enough to provide the threshold condition of intensity, necessary for high-order harmonic production, it can achieve high-order harmonic production by injecting gas atoms into the region where the laser pulse amplification is performed [3]. It should be noted that this process does not require an additional cavity or laser pump to amplify the pulse and also does not reduce the amplified pulse repetition rate [8]. Since the nanostructure shape plays an important role in the heterogeneity of the scattered field around the hot zone (with stronger field amplification) in this study based on the past research in this field [9–11] and in particular, the field of metallic disk nanostructure which placed on the insulation layer and the metal layer ([12]) is investigated.

In order to investigate the heterogeneity and the possibility of high-order harmonic generation, argon gas injected into the hot nanostructured area.

In the above nanostructure, by the interaction between the surface plasmons associated with the coupled nanodisks

✉ Masoud Mohebbi
m.mohebbi@vru.ac.ir

¹ Department of Physics, Faculty of Science, Vali-E-Asr University of Rafsanjan, P.O. Box No: 77139-36417, Rafsanjan, Iran

and the metal layer placed on the insulating layer, significant amplification appears in the electric field of nanostructure band gap. Based on the proper choice of thickness, size and material of the layers, and nanodisks, these properties can be optimized by optimizing the electric field amplification at the desired wavelength, in fact, the central wavelength of the commercial titanium-sapphire laser.

The circular cross-section nanostructures (due to their low curvature) are less reinforced in the near-structure areas than the triangular nanostructures which used in the experiment conducted by Kim and his colleagues [3]. The results of the calculations show that the disk nanostructure changes the direction of electron motion and consequently the electron dynamics, so that, at low intensities, the lasers lead to the emission of photons with higher cutoff frequency. In other words, the heterogeneity of the field in the band gap in the disk nanostructure is less than that of the triangular nanostructure, which behaves almost like a static field. We use metal substrates to overcome the reduction in amplification, which significantly increases the amplitude of the electric field and consequently increases the frequency of the cutoff. Also, due to its circular cross-sectional area, the disk nanostructure is capable of pumping more noble gas atoms into the band gap, which results in higher high-order harmonic generation efficiency.

In the following, first, the field scattering caused by nanostructures is investigated and then, using this field, high-order harmonic generation and attosecond pulse generation are investigated. The nanostructures studied are two nanodisks of the same radius and thickness, which are located on an insulated substrate and a metal film of a certain thickness. The electric field amplification optimized at 800 nm by simultaneously changing the radius of the two nanodisks. The field scattering is also investigated in nanodisks by changing their material, such as gold-silver and silver-silver. Finally, argon-like atoms, similar to the experimental work of Kim and his colleagues, are pumped into the connecting line of optimized nanodisks, and nonlinear response of these atoms to the laser field is investigated.

It should be noted that thermal and nonlinear effects have not been studied in this simulation. Rather, similar to a number of works done in this field, such as [3–6, 9–11], the study is limited to typically plasmonic works.

Scattering of Laser Field by Nanostructure

Gold–Gold Nano Disks

The investigated nanostructure consists of two 5-nm gold disks with a gap of 20 nm located on a 10-nm-thick sapphire insulator and a 5-nm gold metal film. This

nanostructure is located in a vacuum box with dimensions of $400 \times 100 \times 200$ nm.

As shown in Fig. 1, the plane-wave light polarized in x -axis is incident normally from the top to the bottom (z -axis). The driving wavelength is taken to be 300–1500 nm. For the given geometry of a nanostructure, the degree of field enhancement induced by resonant plasmons can be estimated by solving Maxwell's equations numerically [13]. All simulations are performed based on the finite difference method in time domain [14, 15].

The space is divided into small units, typically cubes, called Yee cells. Cell is assigned the susceptibility for a given material. The FDTD method calculates the electric and magnetic fields in each cell by integrating the Maxwell's equations in a “leap-frog” fashion until the steady state is reached.

In order to obtain an accurate field distribution for the three-dimensional object, the cell size must be much less than size of relevant features. In our case, this requires a cell size of 0.5 nm. Such small cells result in extremely short time steps in the simulation, as the FDTD algorithm is stable only if $dt \leq du/(c\sqrt{3})$, where u is the side of a cubical cell. The perfectly matched layers (PMLs) have been applied at the simulation model to reduce reflections from the sides of the simulated space [16].

The wavelength-dependent dielectric constant of the different material in nanostructure was determined using the measured values in the ref [17].

As shown in Fig. 2, the field vector value is calculated and collected in the following cases: (a) point A is located at 1 nm away from the edge of the nanodisk and a height of 2.5 nm (half the thickness of the nanodisk) from the sapphire substrate surface, (b) blue line: the connecting line between two centers of nanodisks at 2.5 nm, (c) green plate: the xy plane located at 2.5 nm (the center of the gap region, and (d) red plate: the xz plane located at the center of the gap region.

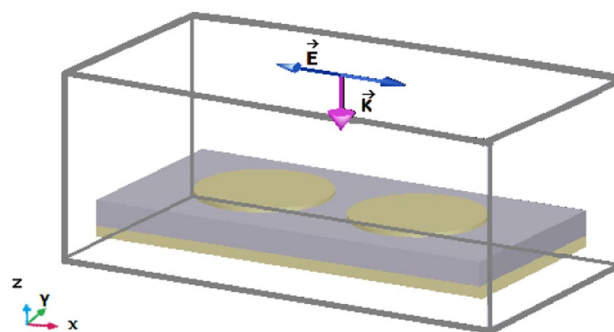


Fig. 1 Three-dimensional schematic diagram of the structure consisting of nanodisks located on the sapphire bed and the gold metal film irradiated in a flat z -plane in the vertical direction z along the x -axis

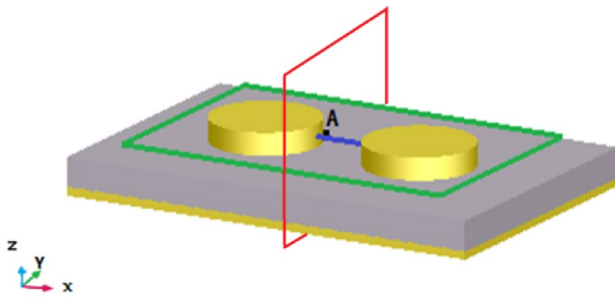


Fig. 2 Illustration of the scattered field collection sites: point at the edge of the nanodisk in half-height (dot A), line from center to center of two nanodisks at half height (blue line), xy (green panel), and xz (red panel) plates mounted at the center of the gap region

First, we investigate the enhancement of the electric field in gold nanodisks having the same geometrical parameters. Two nanodisks of gold are selected with a radius and thickness of 40 nm and 5 nm with a gap of 20 nm, respectively, which are 10 nm and 5 nm thickness, on the substrate and the gold metal film, respectively.

The two-dimensional distributions of the amplified electric field in the xy and xz planes at 800 nm are shown in Figs. 3 and 4. The normal electric field (field enhancement factor) is determined as the amplitude ratio of the scattered local electric field to the incident electric field.

Also, the x-directed, y-directed, and z-directed electric field distributions can be used to determine the distribution of electric fields in the gap region of the coupled metallic nanodisks. According to the figure, the highest amount of scattered field is observed at the surface of nanodisk and at the gap between the two nanodisks along the x-axis.

Normal scattered field at a point in the nanodisk which located at half the height of the disk (2.5 nm height) on its rotating surface (point A shown in Fig. 2) is shown in Fig. 5a versus the wavelength of the incident field. According to the figure, the maximum amplitude of the incident field is 29.55 times at 1124.53 nm. Also, the enhancement of the electric field from the center of one disk to another at a wavelength of 800 nm is shown in Fig. 5b. According to figure, the maximum enhancement factor of 6 times occurs at the edge of the nanodisks.

Since the aim is to achieve the greatest amplification of the electric field at 800 nm (the central wavelength of the sapphire laser), we optimize it by simultaneously changing the radius of the two nanodisks. For this purpose, two nanodisks with radii of 19, 20, and 30 nm with the above-mentioned characteristics are selected and irradiated by laser field in the wavelength range of 300–1500 nm. According to the results in Fig. 6a, a decrease in the nanodisk radius shifts the resonance peaks towards shorter wavelengths and also, a decrease in field amplification is observed due to size effects during light polarization. As the radius increases, the attraction between the dipoles in the nanodisk decreases. This means a decrease in the restoring force which results in a decrease in the resonant frequency (wavelength increase) [18].

Moreover, the amplification of the electric field on the connecting line of nanodisks at half height of them at 800 nm is shown in Fig. 6b. According to the results, nanodisks with a radius of 19 nm (black dot curve) have the highest amplification factor of 51 at 800 nm, which is the optimum radius.

Fig. 3 Normal electric field distribution of two gold nanodisks having a radius and thickness of 40 and 5 nm, respectively, and 20 nm gap based on sapphire substrate and gold metal film with 10 and 2 nm thickness, respectively, at a wavelength of 800 nm on the xy plane

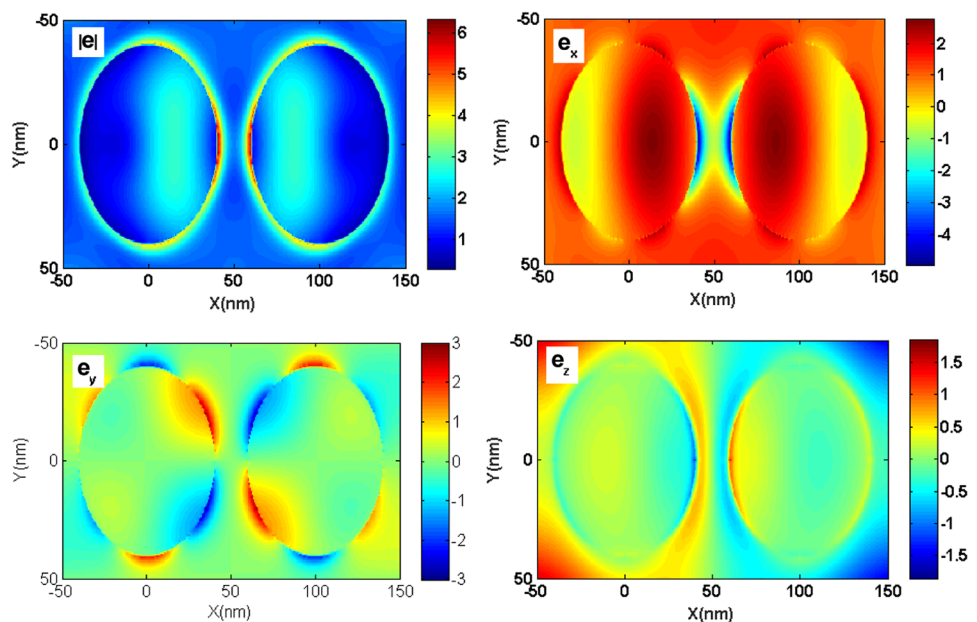
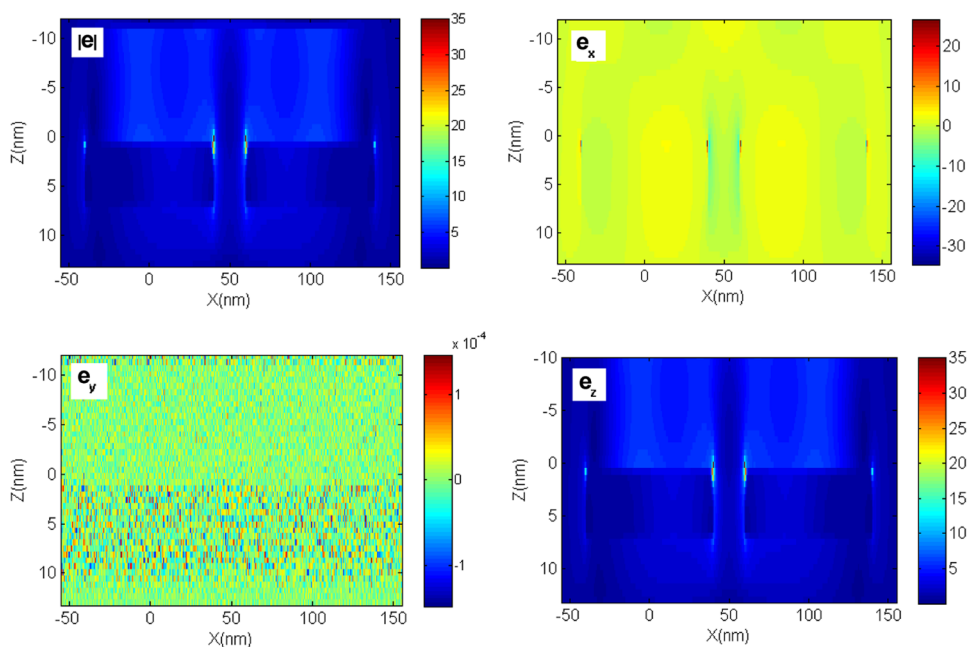


Fig. 4 Normal electric field distribution of two gold nanodisks having a radius and thickness of 40 and 5 nm, respectively, and 20 nm gap based on sapphire substrate and gold metal film with 10 and 2 nm thickness, respectively, at a wavelength of 800 nm on the xz plane



Gold-Silver and Silver-Silver Nanodisks

In this section, the effect of the radius on the field enhancement is investigated by changing the material of the disks. By examining the different radii, the results show that by selecting two identical nanodisks including gold-silver (green-dotted curve) and silver-silver (pink-dashed curve) with the radius of 20 and 22 nm, respectively, the highest amplification is around 800 nm (as shown in Fig. 7a) with the values of 29.1 and 41.8 times at point A (as shown in Fig. 2), respectively. Moreover, in order to compare the enhancement values for the optimum gold-silver and silver-silver with gold-gold (preceding section), the field enhancement for the two optimum gold nanodisks with blue solid curve is shown in Fig. 7a. As can be seen, the gold-gold structure shows a lower enhancement than the gold-silver and silver-silver structure which has a greater radius than the gold-gold structure.

The amplification of the electric field on the connecting line of two nanodisks for the gold-gold, gold-silver, and

silver-silver structures is shown at half the height of the two disks at 800 nm in Fig. 7b. According to the figure, the silver structure (pink-dashed curve) with a larger radius (22 nm) has a highest enhancement on the edges with a value of 86 times at 800 nm.

Analysis

In order to investigate the effect of gold substrate and metal film on electric field amplification, for three nanostructures, the electric field amplification curve versus wavelength at point A is drawn in Fig. 8a:

- 1 Two gold nanodisks (with a radius of 19 nm with a height of 5 nm) placed on the sapphire layer (10 nm thickness) and a gold metal film (5 nm thickness),
- 2 Two gold nanodisks (with a radius of 19 nm with a height of 5 nm) placed on the sapphire layer (10 nm thick) and without gold metal film,

Fig. 5 Electric field amplification for two gold nanodisks having a radius and thickness of 40 and 5 nm, respectively, based on the sapphire substrate and the gold metal film: **a** in the wavelength range 300–1500 nm at point A and **b** on the line of the two nanodisks at the half height of the two disks at 800 nm

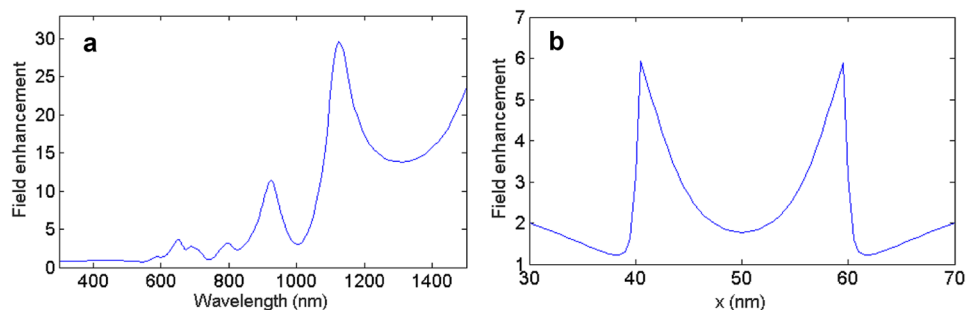
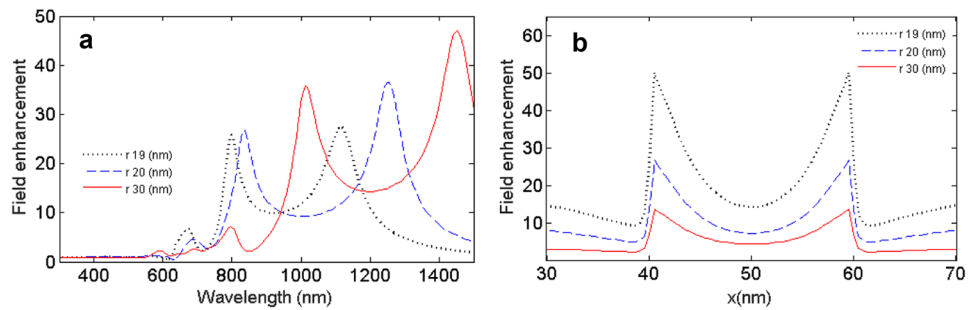


Fig. 6 Electric field amplification for two 5-nm gold nanowires located on the substrate insulation and metal film: **a** in the wavelength range 300–1500 nm at point A at different radii and **b** on the connecting line of nanodisks at the half heights of them at 800 nm for different radii



3 Two gold nanodisks (with a radius of 19 nm with a height of 5 nm) with no gold substrate and gold metal film.

Also, the electric field amplification in the connecting line of nanodisks for the three structures above, at 800 nm, is plotted in Fig. 8b, indicating that the use of insulating substrate and metal film significantly enhances the field strength in comparison with other cases.

According to Fig. 8a, the field amplification curve of two nanodisks with a radius of 19 nm (black curve) has a resonance peak at 608 nm with a value of 10.79 times. When two nanodisks with a radius of 19 nm are placed on the 10 nm insulation substrate (sapphire), an increase in electric field amplification and shift toward longer wavelengths (red shift) is observed. As shown by the blue-dotted curve, the resonance peak lies at 719.8 nm with a value of 16.32. Due to the presence of the insulating substrate, the charge symmetry in the nanostructure is broken and the spectrum usually shows a red shift. More precisely, the optical response of metal nanoparticles to the substrate is still affected by the presence of surface plasmon resonances. The location and width of these resonances depend on the geometry and dielectric properties of the system. When the system is exposed to an external electric field force, charge polarization is created, which causes the charge distribution on the substrate as well as the charge distribution change on the nanoparticles. In the quasi-static range, as shown in Fig. 9a, this redistribution can be due to the distribution

of imaging charge caused by the nanoparticles [19]. By placing nanodisks based on the insulating substrate on a 5-nm metal film, the field amplification increases. When the nanodisks located on the insulation substrate are irradiated by the electric field, the electric field passes through the substrate after interacting with the nanodisks. Whereas the case of in which nanodisks based on sapphire layer and metal film, after creating the charge distribution on the metal film, the electric field energy returns back (towards the nanoparticles) by the propagation modes, after the interaction, it amplifies the electric field [20]. The effect of propagating modes can be statically seen as the presence of imaging charges which caused by nanodisk on the metal site (Fig. 9b). Figure 8 a also shows some resonance peaks (red-dashed curve) due to the activation of the upper and lower dipoles (quadrupole) on the metal film due to the penetration of the field scattered by the nanodisks.

To verify this statement, the depth of penetration (skin depth) for the metal film can be calculated. Depth of penetration as a relation

$$\delta = \frac{\lambda_0}{2\pi \text{Im}(n)} \tag{1}$$

is expressed in [21] that λ_0 is the wavelength of free space and $\text{Im}(n)$ is the imaginary part of the metal complex refractive index which can be calculated from the relation:

$$\text{Im}(n) = \sqrt{0.5(\sqrt{\epsilon''^2 + \epsilon'^2} - \epsilon')} \tag{2}$$

Fig. 7 Electric field amplification for two nanodisks with different material: **a** in the wavelength range 500–1500 nm at point A and **b** in the connecting line of nanodisks at 800 nm

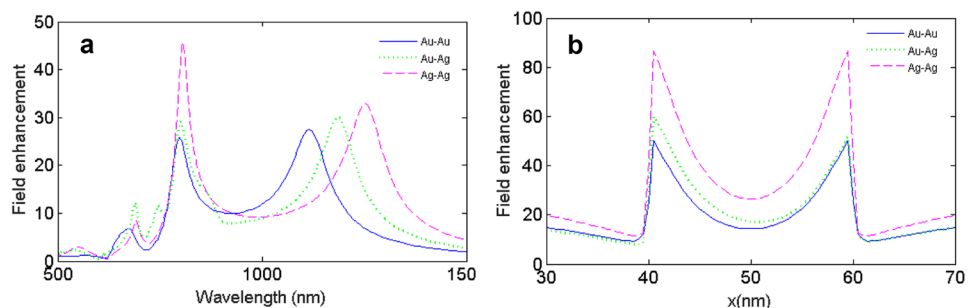
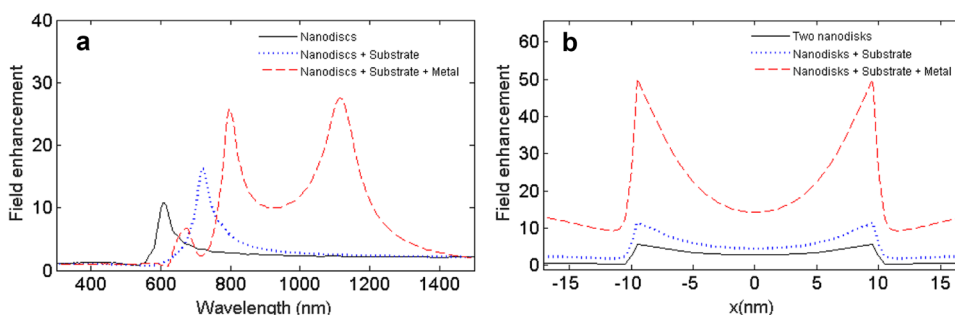


Fig. 8 Electric field amplification for different nanostructures: **a** in the wavelength range 300–1500 nm at point A and **b** two nanodisks at half-height at 800 nm



In relation (2), ϵ' and ϵ'' are the real and imaginary parts of the metal electrical permeability, respectively. For gold, the wavelength of penetration (skin depth) is plotted in Fig. 10. According to the shape of the metal, gold at about 800 nm has a skin depth of about 27 nm.

In gold film with a thickness of 5 nm, which has a thickness less than the penetration depth, the penetration field from nanodisks can excite local charges on the upper surface of the metal film and interact with them. It also penetrates the lower surface of the film and excites local charges there.

Also, for further investigation, one can look at the enhancement mechanisms from another aspect. To do this, the value of scattered field at point A and point B (center of gap at half height) in terms of wavelengths for cases below:

- 1 Two gold nanodisks (with a radius of 19 nm with a height of 5 nm) based on the sapphire layer (with a thickness of 10 nm) with gold metal film (with a thickness of 5 nm),
- 2 Two gold nanodisks (with a radius of 19 nm with a height of 5 nm) located on the sapphire layer (with a thickness of 10 nm) without gold metal film,
- 3 Sapphire layer (with a thickness of 10 nm) and gold metal film substrate (with a thickness of 5 nm),

4 Gold metal film (with a thickness of 5 nm), in the air, is plotted in Fig. 11.

As can be seen, for the gold metal in the air as a rectangular cubic metal nanoparticle, the resonance occurs at approximately 1000 nm. By placing a sapphire layer on this metal film, a red shift for the resonance wavelength appears at approximately 1045 nm. Changing the ambient refractive index (sapphire layer) causes a red shift in plasmonic resonance, which is the presence of a metal-based imaging charge on the sapphire layer.

On the other hand, two gold nanodisks, which are independently placed on the sapphire layer, have only a local plasmon resonance wavelength located at approximately 670 nm. From the interaction between these two independent local plasmonic modes (one, corresponding to the sapphire layer and the metal film substrate and the other, related to the two nanodisks which placed on the sapphire layer, independent from each other), two wavelengths can be expected with the shifted location in accordance with the black-dotted curve.

The field resulting from this interaction varies depending on the location of points A and B. The observed point, the closer the space between the two nanodisks to the surface of the nanodisk, the stronger the field will feel due to the approaching to the surface charge accumulation on the metal surface.

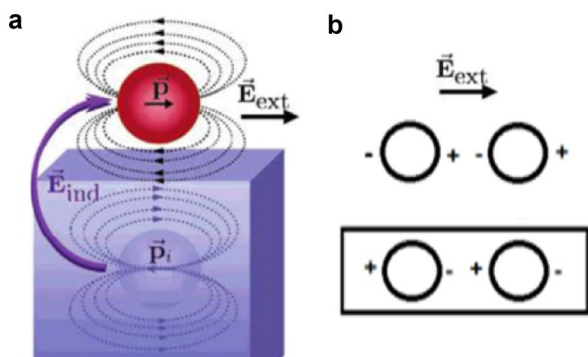


Fig. 9 Schematic diagram showing: **a** the electromagnetic interaction between the nanoparticles and the substrate for the field applied [19] and **b** the interaction of a nanoparticle with a metal surface

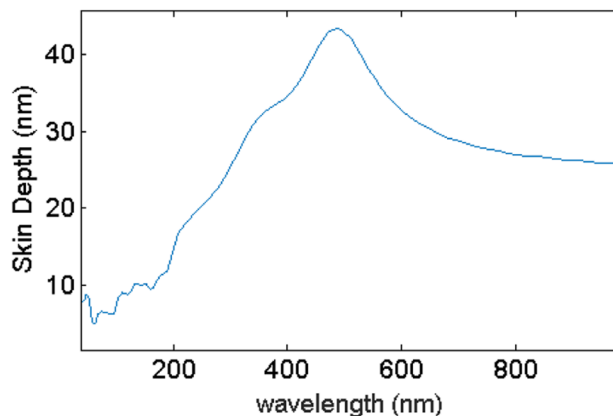
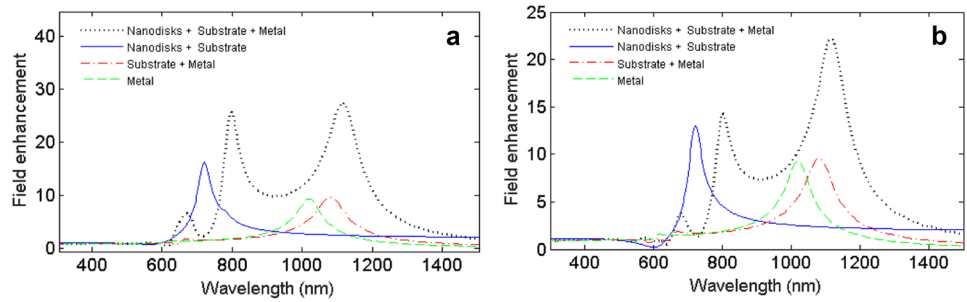


Fig. 10 Skin depth of gold metal versus wavelength

Fig. 11 Electric field amplification for different nanostructures in the wavelength range 300–1500 nm, **a** at point A and **b** B: the midpoint of the two nanodisk gap



High-Order Harmonic Generation Using Amplified Field

Finally, by injecting the argon atom in the middle of the gap at the center of connecting line of two nanostructures at the height of 2.5 nm, one can investigate the nonlinear response of atom to the amplified field. The dynamics of the motion of an electron moving in an electric field (amplified inside the gap at the center of connecting line between two nanostructures at the height of 2.5 nm) with linear polarization can be approximated by solving a time-dependent Schrodinger equation, as follows:

$$i \frac{\partial \psi(x, t)}{\partial t} = \left[-\frac{1}{2} \frac{\partial^2}{\partial x^2} + V_c(x) + V_{\text{int}}(x) \right] \psi(x, t) \tag{3}$$

$$V_c = -\frac{0.775}{\sqrt{1+x^2}} \tag{4}$$

and

$$V_{\text{int}} = -E(x, t)x \tag{5}$$

are coulomb potential and the laser interaction potential, respectively. $E(x, t)$ is the electric field inside the gap of nanostructure at the center of connecting line between two nanostructures at the height of 2.5 nm.

We solve numerically the 1D time-dependent Schrodinger equation using the second-order splitting-operator fast Fourier transform algorithm [22].

According to the Ehrenfest theorem, the time-dependent dipole acceleration can be written in the form

$$a(t) = \langle \psi(x, t) \left| -\frac{d(V_{\text{atom}} + V_{\text{int}})}{dx} \right| \psi(x, t) \rangle \tag{6}$$

The harmonic spectrum can be obtained by the Fourier transformation of $a(t)$:

$$S(\omega) \propto \left| \frac{1}{\sqrt{2\pi}} \int_{-\infty}^{\infty} d_A(t) e^{-i\omega t} dt \right|^2 \tag{7}$$

The temporal profile of an attosecond pulse can be obtained by superposing several harmonics:

$$I(t) = \left| \sum_q a_q e^{iq\omega t} \right|^2 \tag{8}$$

where q is the harmonic order and a_q is the corresponding Fourier transforms.

First, Fig. 12 exhibits the harmonic spectrum generated by the optimal nanostructures whose amplification is shown in Fig. 6. The entire set of nanostructures and argon atoms is irradiated with a laser beam with central wavelength $\lambda = 800\text{nm}$, pulse duration $\tau = 10\text{fs}$, and beam intensity $10^{11} \text{ W cm}^{-2}$. The polarization of the field is linear and is along the line from the center to the center of the two nanodisks (i.e., the x -axis).

The corresponding spectrum with gold–gold, silver–silver, and gold–silver nanostructures has a multi-plateau spectral structure that does not have a clear cutoff frequency. But what is certain is that the corresponding spectrum of silver–silver nanostructures has higher-order harmonics than gold–silver nanostructures, as well as gold–silver nanostructures than gold–gold nanostructures.

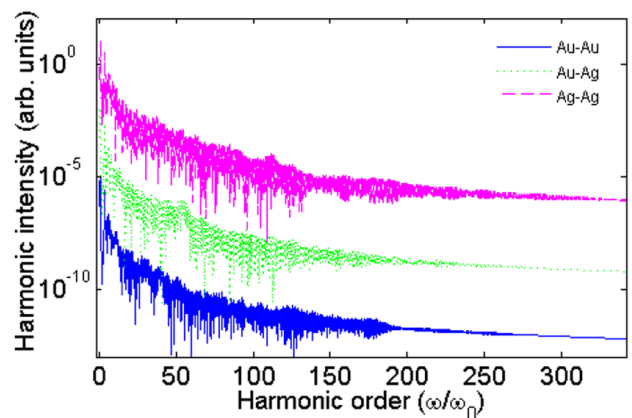


Fig. 12 HHG spectrum produced using the argon atom at the center of the gap of the optimized nanostructures identified in Fig. 6

These effects are related to the electron trajectories that contribute to the harmonic spectrum. Using Gabor analysis [23], the spectral characteristics of HHG and electronic trajectories can be evaluated.

Starting from the dipole acceleration $a(t)$ of Eq. (6), the Gabor transform is defined as

$$a_G(\omega, t) = \int dt' a(t') \frac{\exp[-(t-t')^2/2\sigma^2]}{\sigma\sqrt{2\pi}} \exp(i\omega t') \quad (9)$$

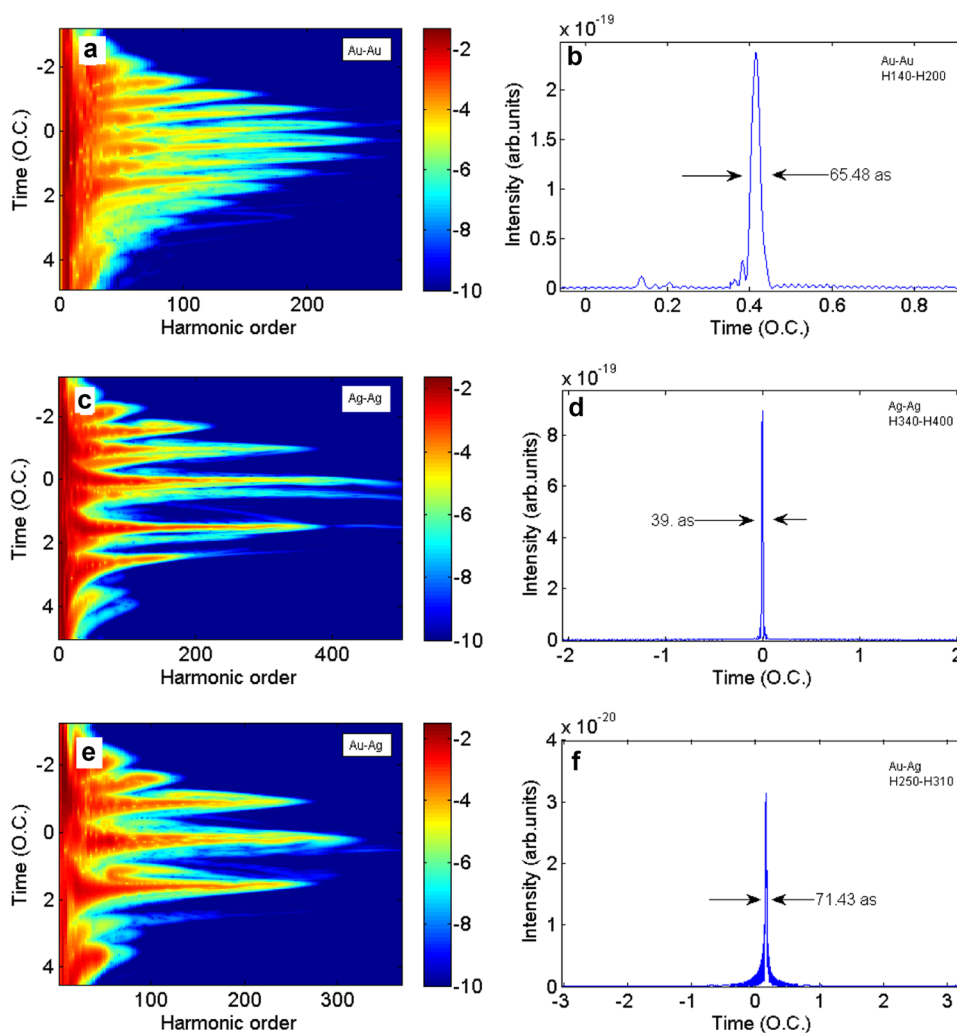
In our studies, we use $\sigma = 1/3\omega$, with ω being the central laser frequency.

The results of the Gabor analysis of the HHG spectra of Fig. 12 are presented in Fig. 13. Figure 13 a presents the time–frequency distribution of the HHG shown by the blue solid curve in Fig. 12. From this figure, one can clearly see that there are five main peaks contributing to the HHG, for the harmonics order above 160th, marked as A, B, C, D, E, F, and G with the maximal harmonic orders of 150, 197, 227, 246, 225, 194, and 155, respectively. For each peak,

two branches exist, the negative slope branch (the long quantum path) and the positive slope branch (the short quantum path). Furthermore, for the harmonics order above 140th, the positive slope branch of the peak D has main contribution in HHG spectrum. This indicates that the positive quantum path control can be achieved in this case. Thus, the harmonics order above 140th becomes smooth but much less modulated. Such a broad supercontinuum is highly likely to support the generation of an isolated short attosecond pulse. Figure 13 b shows the temporal profile of the as pulse by filtering the 140th–200th harmonics. As shown in this figure, a single 65.48 as pulse with a small satellite is obtained. The intensity of the satellite pulse is approximately 18 times lower than that of the main pulse.

Figure 13 c presents the time–frequency distribution of the HHG shown by the pink-dashed curve in Fig. 12. From this figure, one can clearly see that there are three main peaks contributing to the HHG, for the harmonics order above 200th, marked as A, B, and C with the maximal harmonic orders of 350, 500, and 390, respectively. In the peak

Fig. 13 Time–frequency distributions of the HHG and temporal profiles of the attosecond pulse by superposing the selected harmonics corresponding to the blue solid, pink-dashed, and green-dotted curves in Fig. 12



B, the long and short quantum paths split in wide range of the spectrum and the harmonic intensity of the long quantum path is lower than that of the short quantum path. We note that both the long and short quantum paths emit rapidly. Furthermore, for the harmonics order above 340th, the peaks A and C have no contribution. From Fig. 13d, one can clearly see that an isolated and shorter 39 as pulse is generated by superposing the harmonics from 340 to 400th order.

Finally, Fig. 13e presents the time–frequency distribution of the HHG shown by the green-dotted curve in Fig. 12. From this figure, one can clearly see that there are three main peaks contributing to the HHG, for the harmonics order above 110th, marked as A, B, and C with the maximal harmonic orders of 245, 310, and 250, respectively. In the peak B, the harmonic intensity of the long quantum path is lower than that of the short quantum path. Furthermore, for the harmonics order above 250th, the peaks A and C have no contribution. From Fig. 13f, one can clearly see that an isolated 71 as pulse is generated by superposing the harmonics from 250 to 310th order. By using the optimized and symmetric nanoantenna, clean and short isolated attosecond pulse with high signal-to-noise ratio is straightforwardly obtained without any phase compensation.

Conclusions

We investigated the field enhancement in the isolated nanostructure consisting of a symmetric and coupled metal disk, an insulator spacer, and a gold film. Results show that a strong coupling between the localized surface plasmon (LSP) on the metal nanoparticles and on the metal film strongly enhances the near-field inside the gap region. By optimizing the design of the nanostructures, the resonant spectra of the nanostructures can support a resonant spectrum with center wavelength of 800 nm (output from a typical Ti: sapphire femtosecond oscillator) and achieve a maximum enhancement up to 86 and an enhancement of 35 in a volume of $15 \times 15 \times 30 \text{ nm}^3$, which is sufficient to enhance the incident radiation to $10^{14} \text{ W cm}^{-2}$. Our calculated results also show that, by adding these nanostructures to the HHG process with argon at a proper scheme, the enhancement of the high-order harmonics and an XUV supercontinuum is observed, and the selection of the short quantum path can be achieved, then an isolated attosecond pulse as short as 39–72 is generated.

The plasmonic nonlinear behavior of metal nanodisks will lead to the emission of a second-order local harmonic field. Due to the low second-order harmonic intensity compared with the amplified base field (the scattered from nanodisks with the same wavelength of the driving field), this component of the scattered field cannot play a role in the nonlinear response of argon atoms to the amplified base field.

Therefore, the accuracy of the results related to harmonic and attosecond pulse generation can remain valid. From an experimental point of view, the thin film nanodisks began to degrade, not abruptly, but starting gradually then continuing at a fast rate, soon after being exposed to the driving laser set to 0.1 TW cm^{-2} intensity. With an acceptable approximation, it can be said that in the absence of heat calculations, the structure does not melt for a limited time. In other words, the results of the calculations are acceptable for this limited time with a good approximation.

Authors' Contributions All authors have participated in (a) conception and design or analysis and interpretation of the data; (b) drafting the article or revising it critically for important intellectual content; and (c) approval of the final version.

Funding No funding was received to assist with the preparation of this manuscript.

Data Availability The datasets generated during and/or analyzed during the current study are available from the corresponding author on reasonable request.

Compliance with Ethical Standards

Conflict of Interest The authors declare that they have no conflict of interest.

Ethical Approval Not applicable.

Consent to Participate Informed consent was obtained from all authors.

Consent to Publish The authors confirm that there is informed consent to the publication of the data contained in the article. We confirm that this work is original and has not been published elsewhere, nor is it currently under consideration for publication elsewhere.

References

1. Du H, Wang H, Hu B (2010) Isolated short attosecond pulse generated using a two-color laser and a high-order pulse. *Phys Rev A* 81:063813. <https://doi.org/10.1103/PhysRevA.81.063813>
2. Corkum PB (1993) Plasma perspective on strong field multiphoton ionization. *Phys Rev Lett* 71:1994. <https://doi.org/10.1103/PhysRevLett.71.1994>
3. Kim S, Jin J, Kim YJ, Park IY, Kim Y, Kim SW (2008) High harmonic generation by resonant plasmon field. *Nature* 453:757–760. <https://doi.org/10.1038/nature0701>
4. Park IY et al (2011) Plasmonic generation of ultrashort extreme-ultraviolet light pulses. *Nat Photonics* 5:677–681. <https://doi.org/10.1038/nphoton.2011.258>
5. Ebadian H, Mohebbi M (2017) Extending the high-order-harmonic spectrum using surface plasmon polaritons. *Phys Rev A* 96:023415. <https://doi.org/10.1103/PhysRevA.96.023415>
6. Ebadian H, Mohebbi M (2018) Plasmonic nanostructure assisted HHG in NIR spectrum and thermal analysis. *J Phys D: Appl Phys* 51:075307. <https://doi.org/10.1088/1361-6463/aaa651>

7. Kelly KL et al (2003) Optical properties of the metals nanoparticles: the influence of size, shape and dielectric environment. *J Phys Chem B* 107:668–677. <https://doi.org/10.1021/jp026731y>
8. Protopapas M et al (1997) Atomic physic with super-high intensity lasers. *Rep Prog Phys* 60:389–486. <https://doi.org/10.1088/0034-4885/60/4/001>
9. Ebadian H, Mohebbi M (2016) Strong electric field enhancements in asymmetric metallic nanostructures and high-order harmonic generation. *Appl Opt* 55(28):8035–8041. <https://doi.org/10.1364/AO.55.008035>
10. Mohebbi M, Nazarpour Malaee S (2015) Electron path control of high-order harmonic generation by a spatially inhomogeneous. *J Mod Opt* 63:643–652. <https://doi.org/10.1080/09500340.2015.1088586>
11. Hekmatara SH, Mohebbi M, Rahpeyma J (2014) Extension of high-order harmonic generation cutoff via control of chirped laser pulses in the vicinity of metal nanostructure media. *RSC Adv* 4:59064–59070. <https://doi.org/10.1039/C4RA08052A>
12. Chu Y, Crozier KB (2009) Experimental study of the interaction between localized and propagating surface plasmons. *Opt Lett* 34(3):244–246. <https://doi.org/10.1364/OL.34.000244>
13. Bohn LJ, Nesbitt JD, Gallagher A (2001) Field enhancement in apertureless nearfield scanning optical microscopy. *J Opt Soc Am A* 18:2998–3006. <https://doi.org/10.1364/JOSAA.18.002998>
14. Taflove A, Brodwin ME (1975) *IEEE Trans Microwave Theory Tech* 23:623–630. <https://doi.org/10.1109/TMTT.1975.1128640>
15. Kunz KS, Luebbers RJ (1993) *The finite difference time domain method for electromagnetics*. CRC, Boca Raton, FL
16. Sabaawi AMA, Tsimenidis CC and Sharif BS (2012) Bow-tie nanoarray rectenna: Design and optimization 6th Eur. Conf. on Antennas and Propagation (EUCAP): 1975–1978
17. Polyanskiy MJ (2014) accessed. <http://www.RefractiveIndex.info>
18. Rechberger W et al (2003) Optical properties of two interacting gold nanoparticles. *Opt Commun* 220:137–141. [https://doi.org/10.1016/S0030-4018\(03\)01357-9](https://doi.org/10.1016/S0030-4018(03)01357-9)
19. Noguez C (2007) Surface plasmons on metal nanoparticles: the influence of shape and physical environment. *J Phys Chem C* 111(10):3806–3819. <https://doi.org/10.1021/jp066539m>
20. Stuart HR, Hall DG (1998) Enhanced dipole-dipole interaction between elementary radiators near a surface. *Phys Rev Lett* 80:5665. <https://doi.org/10.1103/PhysRevLett.80.5663>
21. Wooten F. *Optical properties of solids*. Academic Press; 1972
22. Feit MD (1982) Solution of the Schrödinger equation by a spectral method. *J Comput Phys* 47:412–433. [https://doi.org/10.1016/0021-9991\(82\)90091-2](https://doi.org/10.1016/0021-9991(82)90091-2)
23. Chirila CC et al (2010) Emission times in high-order harmonic generation. *Phys Rev A* 81:033412. <https://doi.org/10.1103/PhysRevA.81.033412>

Publisher's Note Springer Nature remains neutral with regard to jurisdictional claims in published maps and institutional affiliations.